

# Influence of cooling rate on microsegregation behavior of magnesium alloys

<sup>1</sup>Md. Imran Khan,<sup>1</sup>Ahmad O. Mostafa,<sup>2</sup>Mohammad Aljarrah, <sup>3</sup>Elhachmi Essadiqi,  
<sup>1</sup>Mamoun Medraj

<sup>1</sup>Mechanical and Industrial Engineering Department, Concordia University, 1455 de  
Maisonneuve Blvd. West, Montreal, Quebec, H3G 1M8, Canada

<sup>2</sup>Industrial Engineering Department, The Hashemite University, P.O. Box: 330127, Zarqa  
13115, Jordan

<sup>3</sup>Renewable Energy & Advanced Materials Research Lab., Université Internationale de  
Rabat, Technopolis, Roccade Rabat - Salé El Jadida, Morocco

Tel: (514) 848 2424 ext. 3146

Fax: (514) 848 – 3175

Corresponding author: mmedraj@encs.concordia.ca

## Abstract:

The effect of cooling rate on microstructure and microsegregation of three commercially important magnesium alloys was investigated in the current research. Wedge ('V' shaped) castings of AZ91D, AM60B and AE44 alloys were made using a water-cooled permanent copper mold to obtain a range of cooling rates from a single casting. Variation of microstructure and microsegregation was studied using a combination of experiments. Chemical composition of alloying elements at the dendritic length scale and different cooling rates was examined using scanning electron microscopy. Solute redistribution profiles were drawn from the experimentally obtained data. Microstructural and morphological features such as dendrite arm spacing and secondary phase particle size were also analyzed using both optical and scanning electron microscopy. Dendrite arm spacing and secondary phase particle size have an increasing trend with decreasing cooling rate for the three alloys. Area percentage of secondary phase particles decreased with decreasing cooling rate for AE44 alloy. The trend was different for AZ91D and AM60B alloys, for both alloys, area percentage of  $\beta$ -Mg<sub>17</sub>Al<sub>12</sub> increased with decreasing cooling rate up to location 4 and then decreased slightly. The tendency for microsegregation was more severe at slower cooling rates, possibly due to prolonged back diffusion. At slower cooling rate, the minimum concentration of aluminum at the dendritic core was lower compared to faster cooled locations. The segregation deviation parameter and the partition coefficient were calculated from the experimentally obtained data.

**Keywords:** Mg-Alloys, AZ91D, AM60B, AE44, microsegregation, equilibrium cooling, Scheil-Gulliver model, Brody-Fleming model

## 1. Introduction

Environmental concern was the key motivating factor behind development of Mg alloys. Better aerodynamic design of ~~the~~ vehicles or engines with improved combustion efficiency can lessen fuel consumption but weight reduction seems to be the most effective way to achieve a substantial fuel saving [1, 2]. Magnesium, with density of  $1.74 \text{ g/cm}^3$ , is the lightest of all the engineering structural metals [3]. Mg-based alloys have an excellent combination of properties which justifies their usage in transportation applications. These properties include excellent strength-to-weight ratio, good fatigue and impact strengths, and relatively large thermal and electrical conductivities [4].

All ~~the~~ commercial magnesium alloys are multicomponent and form a variety of phases during solidification and subsequent processing stages. High-pressure die casting and gravity casting, particularly sand and permanent mold casting are the common casting processes used to produce Mg alloy components. Other pertinent production technologies include: squeeze casting, thixocasting and thixomolding [5]. The wide ranges of operational conditions existing in foundry and casting processes generate, as a direct consequence, a diversity of solidification microstructures. Because microstructure determines the final properties of the material, proper understanding of the microstructure formation mechanisms is extremely important. Mechanical properties depend on the microstructural arrangement defined during solidification such as the amount and distribution of eutectic phases, grain size, dendrite spacing, and porosity [6]. Segregation or redistribution of solutes during solidification is closely linked with dendrite arm spacing, inter-dendritic porosity, and the amount and distribution of eutectic phases. The mechanism of microsegregation during solidification of aluminum alloys has received considerable attention but microsegregation during solidification of magnesium alloys has not been systematically studied. To understand the influence of cooling rate on microsegregation of magnesium alloys, this work aims to carry out an experimental investigation using wedge cast samples of AZ91D, AM60B and AE44 alloys. By applying the wedge casting solidification technique, it is possible to produce a range of cooling rates in one casting.

## 2. Literature data

Very few experimental works [7-10] regarding the microsegregation analysis of magnesium alloys were found in the literature. In contrary, several studies [11-20] were carried out to investigate the solidification behavior of magnesium-based alloys. Although the prime focus of these studies ~~were~~ was not on microsegregation analysis but valuable information regarding

elemental composition at different cooling rates and conditions could be obtained from them. Mirković et al. [8, 9] studied the microsegregation of AZ31 and AM50 alloys, applying directional solidification technique. They reported that the segregation behavior of manganese is opposite compared to both aluminum and zinc. This can be explained by understanding the ternary Mg-Al-Mn system, where the Mn forms a peritectic system. Peritectic systems are known to show reversed segregation. Zhang et al. [10] studied the microsegregation in directionally solidified Mg-4Al binary alloy. They determined microsegregation in specimens directionally solidified with cooling rates ranging from 0.06 to 0.8K/s. They reported that the concentration profile of Al at high growth rate or higher cooling rate is closer to the Scheil model. Zheng et al. [7] investigated the microsegregation pattern of Mg-4Al-4Ca alloy under different growth rates using the directional solidification technique. They suggested that the Scheil model can be used in microstructure simulation of this alloy as the microsegregation of the alloying elements (Al and Ca) predicted by this model agreed reasonably well with the EPMA measurements.

Wei et al. [21] carried out microstructural characterization of several magnesium alloys in the AM series in as-cast condition. They performed quantitative analysis of the Al segregation in the die cast alloys by examining thin foil specimens in the TEM. Compositional measurements across an  $\alpha$ -Mg grain in AM50A at intervals of 180 nm were performed using X-ray energy dispersive spectrometry (EDS) in the TEM along a straight line. They found that the Al composition in the interior of Mg grain was approximately 1.5 wt.% which increased to 3.0 wt.% in the area adjacent to the grain boundaries. They repeated the same procedure for a thin foil sample of die cast AM60A at intervals of 600 nm. The Al content varied from 2 wt.% in the grain interior to approximately 4 wt.% in the Al-rich grain boundary region. The width of the high Al region was about 2–3  $\mu$ m. They also reported that owing to the low Al content, no  $\beta$ -Al<sub>12</sub>Mg<sub>17</sub> formed in AM20 but there was intergranular Al segregation.

Barbagallo et al. [19] determined the variation of the alloying element contents through the grain boundaries of an HPDC AM60 alloy by means of EPMA line scanning and reported that the Al concentration varied from 2.5 wt.% in the bulk  $\alpha$ -Mg core to 10 wt.% in the boundary region. It is to be noted that for the same alloy AM60, Wei et al. [21] and Barbagallo et al. [19] reported different amount of Al content in the grain boundary region, this is due to the fact that the casting conditions of the samples were different. Han et al. [22] reported that for permanent mold casting of AZ91D alloy, in the dendritic center the aluminum concentration is 2.6wt.% but it is

11.7wt.% at the dendrite edge, about 4.5 times higher than that in the dendrite center. Zhang et al. [23] conducted experiments to compare the amount of microsegregation in permanent mold cast and die-cast AZ91 alloys. They reported that the average concentration of Al and Zn is lower in the die casting matrix than in the permanent mold casting matrix. Average concentration of Al is 3.3wt.% and for Zn it is 0.33wt.%, in permanent mold casting and 3wt.% Al and 0.22wt.% Zn in die-cast matrix, which means the amount of segregation was higher for comparatively faster cooling. Ditze et al. [24] reported for strip casting of AZ91 alloy, the aluminum content increased from 1 wt.% at the center of the dendrite arms where solidification had started to about 2.5 wt.% between the arms where solidification had ended. Guo et al. [25] reported that in AZ80 alloy the regions close to the  $\beta$ -Mg<sub>17</sub>Al<sub>12</sub> eutectic phase have higher aluminum contents, the maximum concentration in the dendritic interstice varied between 6.6 wt.% and 7.9 wt.%. They also reported that applying electromagnetic vibration on the billet, they could increase the value of minimum Al concentration up to 3.5 wt.% from 2.5 wt.%, which is the minimum concentration of Al in the  $\alpha$ -Mg matrix in the center ~~in-ofa~~ conventional die-cast billet. That means that they could reduce the amount of microsegregation by agitating the liquid. Table 1 summarizes the available data from the literature.

**Table 1: Summary of the literature data**

Alloy	Casting condition	Min. Al wt. %	Max. Al wt. %	Scheil model		Ref.
				Min. Al wt. %	Max. Al wt. %	
Mg-4Al-4Ca	DS*	1	>3	1	3	
AZ31	DS	1	4-5	1	>6	[7]
AM50	DS	<2	8-9	<2	>10	[8, 9]
Mg-4Al	DS	< 2	8-9	<2	>10	
AM60	HPDC**	2.5	10	-	-	[10]
AM50A	Die casting	1.5	3.0	-	-	[19]
AM60A	Die casting	2	4.0	-	-	[21]
AZ91D	PMC***	2.6	11.7	-	-	
AZ91D	PMC	3.3	-	-	-	[22]
AZ91D	Die casting	3	-	-	-	[23]
AZ91D	Strip casting	1	2.5	-	-	
AZ80	Die cast billet	2.5-3.5	6.6-7.9	-	-	[24]

\* DS: directional solidification; \*\* HPDC: high-pressure die casting; \*\*\* PMC: permanent mold casting

Segregation takes place due to unequal solute diffusion rates in the solid and the liquid phases of the solvent material. As a result, the phases that solidify in the later stages of the solidification process, such as  $\beta$ -Mg<sub>17</sub>Al<sub>12</sub>, are placed between dendrite arms. Gungor [26] reported that the extent of microsegregation in an alloy could be determined experimentally by measuring one of

the following: amount of nonequilibrium eutectic, amount of nonequilibrium second phase, minimum solid composition, ratio of minimum and maximum composition of the primary phase, and composition versus fraction solid profile. Experimental techniques to investigate the extent of microsegregation include quantitative metallography (point count, areal, and lineal measurements), X-ray diffraction analysis[27] and electron microprobe measurements.

Of the techniques available, the most widely used for characterizing microsegregation is the random sampling approach developed by Flemings et al.[28], commonly known as the point matrix or area scan approach. There is no hard and fast rule about the total number of points to be taken to represent the compositional variability. Gungor[26] reported that at least 100 points are necessary to obtain a reasonably accurate result. He showed that the result did not vary significantly if 300 points are taken instead of 100 points. These points are acquired by means of scanning electron microscope–energy dispersive spectroscopy (SEM–EDS) or electron microprobe analysis using wavelength dispersive spectrometry (EPMA–WDS). ~~Other~~ Two comparatively less applied methods are compositional maps and segregation ratio. With compositional maps it is possible to present the nature and variability of the dendritic structure and associated microsegregation, but it is not a suitable method for comparing different samples.

~~Segregation~~ The segregation ratio usually refers to the maximum over minimum or the maximum over bulk composition. These are the simplest parameters for comparing different samples but much information is lost. Martorano et al. [29] used a refined segregation ratio, the average deviation between the measurements and nominal composition were reported.

Two approaches were suggested to sort the EPMA data points into increasing or decreasing order depending on their segregation behavior to produce composition versus solid fraction profiles for each element. These approaches are, sorting all the measurements based on composition of a single component (single-element sorts) or sorting based on the compositional difference between two solutes (difference sorts). Yang et al. [30] reported that sorting based on primary alloying elements can produce more accurate elemental partition coefficients. However, the main weakness of both techniques lies in the appropriateness of the choice of the elements upon which to base the sort; for a 10-component alloy, there are 90 different permutations of the difference sorts to consider[31].

Ganesan et al. [31] proposed an alloy-independent sorting algorithm. They termed it weighted interval ranking sort (WIRS). In this approach, all elements present at each data point are considered along with the measurement errors accrued during data treatment. By applying this

approach for segregation profiling of Ni-based alloys, they demonstrated that this sorting method treats eutectic constituents appropriately and ~~noise-the errors~~ in the segregation profile ~~is-are~~ also more accurately ~~distributed~~ determined. The WIRS method was applied in this work as this alloy independent sorting method could accurately treat the eutectic constituents of the three investigated multicomponent alloys.

Segregation ratio and segregation index: these two methods rely on the minima or maxima of an alloying element at a particular location to calculate segregation severity. These calculations might be sometimes misleading ~~sometimes~~ as only the terminal points of solute profiles are being considered instead of the entire variation. Poirier [32] proposed the segregation deviation parameter method for measuring the severity of microsegregation. This method is better in the sense that the deviation is calculated over the entire range of data.

$$\sigma_m = \frac{1}{nC_0} \sum_{i=1}^n |C_i - C_0| \quad 1$$

In this method, the segregation deviation parameter,  $\sigma_m$  is calculated using Equation 1. The absolute difference between the composition at any point  $C_i$  and the bulk composition  $C_0$  is measured and the sum is taken for all the readings. Then, this summation is divided by the total number of points analyzed and the bulk composition.

Both the segregation deviation parameter and the segregation index were employed in this work to compare the severity of microsegregation at different locations of the wedge cast samples.

### 3. Analytical microsegregation modeling

Several analytical microsegregation models [27, 33-38] have been found in the literature to model the solute redistribution of alloying elements during dendritic solidification of alloys. In most of the models, mass balance for the solute elements is considered within a simplified geometry such as a plane, cylinder or sphere to describe the growth of dendrite arms. It is obvious from theoretical and experimental evidences that the simplified geometry gives reasonably accurate results for the majority of ~~the~~ alloy systems and solidification processes [39-41]. The simplest formulations are the equilibrium solidification model (lever rule) and Scheil-Gulliver model, which describe the two extreme cases of ideal equilibrium and non-equilibrium, respectively. With the advent of more sophisticated computing technology and improvement of material databases, the more advanced models (Kraft [40], Du [42], Boettinger[43]) incorporate more realistic variable diffusion properties across the solid-liquid interface. Three models will be

described in the following section: Equilibrium solidification model, Scheil-Gulliver solidification model and Brody-Flemings dendritic solidification model.

### 3.1 Equilibrium solidification model

This model assumes that a state of equilibrium exists at the solid-liquid interface during growth. That means there would be negligible resistance for transportation of atoms between the solid and liquid phases[44]. For instance, if a single crystal of alloy composition  $C_0$  is cooled to temperature ( $T^*$ ), which is below the liquidus temperature ( $T_L$ ), then according to the equilibrium solidification theory,  $C_L^*$  and  $C_S^*$  would be the respective compositions of liquid and solid at the interface. The partition coefficient  $K$  is the ratio of the composition of the solid to that of the liquid. It indicates the degree of segregation of solute. The equilibrium partition ratio may be defined as:

$$K = \frac{C_S^*}{C_L^*} \quad 2$$

A value less than unity indicates that the element is partitioning preferentially to the eutectic region whereas a value greater than unity indicates that the element is partitioning to the dendrite core as peritectic solidification. The farther from unity the partition coefficient is the more strongly the element partitions to either the dendrite core or eutectic region. Physical parameters that contribute to the partitioning coefficient are differences in atomic radii (the tendency for an element to be in solution) and the chemical potential of the elements in the liquid.

Applying the equilibrium lever rule the amount of solute redistribution during equilibrium solidification can be determined by:

$$C_S f_S + C_L f_L = C_0 \quad 3$$

Here  $f_S$  and  $f_L$  are weight fractions of solid and liquid respectively. The above equation can be written in the following form:

$$C_S = \frac{K \cdot C_0}{(1 - f_S) + K \cdot f_S} \quad 4$$

This equation describes the composition of the solid phase with respect to the fraction of solid. Where,  $C_S$  is solute concentration in the solid (wt.%),  $C_0$  is the initial solute concentration (wt.%),  $K$  is the partition coefficient, and  $f_S$  is the fraction solid.

According to the assumption of the equilibrium model, there would be complete diffusion in the liquid and solid phases that means the final product would have a homogeneous composition  $C_S = C_0$ [44].

The dependency of liquidus temperature on the changing liquid composition would result in solidification of the alloys over a range of temperature. The first solid would start forming and the composition would be lower in solute, for eutectic alloys, compared to initial liquid composition. As the solidification progresses, the balance of the solute would be rejected enriching the liquid through diffusion. This would eventually result in lower liquidus temperature than that of the initial composition. This solute rejection process is liable-responsible for the development of segregation or coring. As a general rule, it can be stated that if the freezing range is larger for an alloy and it gets sufficient time for solute rejection, the segregation severity would be more [45].

### 3.3 Scheil-Gulliver solidification model

This model is different from the equilibrium model in the sense that it does not allow any elemental diffusion in the solid. That means, once a solid is formed nothing comes out of it or gets in. This would result in a steady rise in rejected solute level in the liquid phase until the final liquid region has reached the eutectic composition. The famous “non-equilibrium lever rule” or more popularly known as the Scheil equation, is as follows:

$$C_S = K \cdot C_0 (1 - f_S)^{K-1} \quad 5$$

### 3.4 Brody-Fleming dendritic solidification model

The work of Brody and Flemings[35] pinpointed the reason for the discrepancy between experimental microsegregation measurements and the values predicted by the Scheil model. This mismatch is due to the presence of finite solid-state diffusion in actual castings, whereas the Scheil model assumes no diffusion in the solid state. Therefore, the amount of back diffusion that takes place, both during and after the solidification, has to be taken into consideration. This back diffusion is liable-responsible for lower solute levels than the prediction of the Scheil model. The extent of back diffusion is determined by the dimensionless parameter,  $\alpha$ , as shown in the integration of the differential solute balance equation for a parabolic growth rate as follows,

$$C_S = KC_0 [1 - (1 - 2\alpha K) f_S]^{(K-1)/(1-2\alpha K)} \quad 6$$

where,

$$\alpha = \frac{4D_S t_f}{\lambda^2}$$

Here,  $D_S$  is the diffusivity in solid ( $m^2 \cdot s^{-1}$ ),  $t_f$  is the local solidification time(s), and  $\lambda$  represents the secondary dendrite arm spacing (m). Equation 6 contains two limiting cases that



were described earlier for plane front solidification, when  $\alpha$  is set to 0.5, then the equation represents the equilibrium lever rule and when  $D_S$  is set to zero (i.e. no solid state diffusion),  $\alpha$  becomes zero, and that results in [the](#) Scheil equation.

There are many other models available in the literature, and the quest for achieving a perfect model is still going on. But, most of these models are modifications of [the](#) Brody-Flemings model. Kearsey[46] in his thesis came to the conclusion that it is really difficult to make accurate microsegregation prediction using these simplified models, as these models do not take into account the complexity regarding the number of diffusing solute species and their relative interactive effects that takes place during the solidification of multicomponent alloys.

#### 4. Methodology

The ingots of the three alloys were melted and ~~de gassing de gassed procedure was carried out~~ using hexachloroethane ( $C_2Cl_6$ ). The pouring temperature of the molten metal in the mold was 1000K or 723°C. Six K-type thermocouples at different locations [along of](#) the wedge casting were placed, as illustrated in Figure 1 (a). Time-temperature curves were obtained at ~~those~~ [each](#) locations using the thermocouple reading. The thickness increases gradually from 6mm at location 1 to 34mm at location 6 as shown in Figure 1 (b). It is expected that location 1 ~~faces~~ [has](#) the fastest cooling rate while location 6 ~~faces has~~ [the](#) slowest cooling ~~among rate of~~ the six locations.

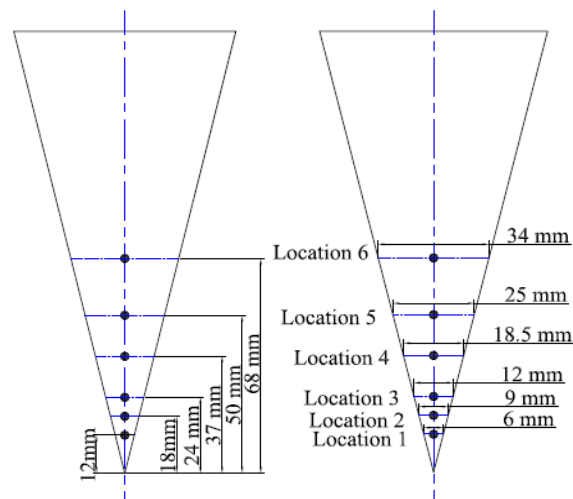


Figure 1: Schematic of thermocouple positions in the wedge cast sample

~~Bulk~~ [The bulk](#) compositions of the investigated alloys ~~is are~~ presented in Table 2. In AE44 alloy, rare earth elements were added as mischmetal. ~~Percentage~~ [The percentage](#) of [the](#) rare earth

elements in the mischmetal is as follows: %Ce=55.90, %La=30.50, %Pd=6.80, %Nd=5.20, % others=1.60.

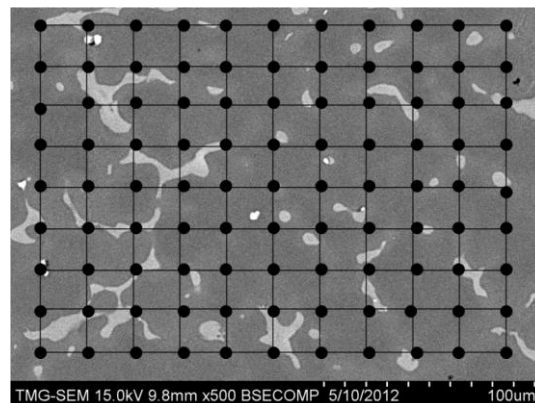
**Table 2: Bulk composition of the investigated alloys (wt.%)**

Alloy	% Al	% Zn	% Mn	% Si	% Cu	% Fe	% Ce (% RE*)
AE44	3.95	0.19	0.3	0.007	<0.005	<0.005	2.20 (3.94*)
AM60B	5.7	0.023	0.31	0.013	<0.005	<0.005	
AZ91D	8.8	0.75	0.34	0.015	<0.005	<0.005	

\* Percentage of the other rare earth elements in the mischmetal

Solidified samples were sectioned longitudinally at the position of the thermocouple s. Samples were ground using 120, 240, 320, 400, 600, 800 and 1200 grit SiC emery paper while ethanol was used as lubricant and the samples were ultrasonically cleaned in ethanol between steps to remove any residue. Samples were etched with nitric acid reagent (20 ml acetic acid, 1 ml HNO<sub>3</sub> (concentrated), 60ml ethylene glycol, 20 ml water) after being manually polished. The solidification microstructures were analyzed by optical microscopy (OM). The phase analyses were investigated using scanning electron ~~microscope~~-microscopy (SEM) (Model, Hitachi S-3400N SEM) equipped with ~~WDS~~ (~~wavelength dispersive spectrometry~~) (WDS) and ~~EDS~~ (~~energy dispersive spectrometry~~) (EDS) systems for elemental analysis. For the SEM, the samples were not etched.

The SEM was used mainly in the backscatter electron (BSE) mode at 15 keV. BSE images were treated ~~in-an~~by image ~~analyzing~~-analysis software in order to enhance the color contrast. The composition measurements for elemental analysis were carried out using EDS. At each sample location, a minimum of 150 readings were taken in a matrix using EDS spot analysis, as shown in Figure 2.



**Figure 2: Schematic of area scan method using EDS. Each black dot corresponds to a composition measurement**

X-Ray Diffraction (XRD), using X'Pert PRO, manufactured by PANalytical Inc., was performed to detect the phases present in these alloys and measure the volume fraction of the dominant secondary phases. The samples' powders were prepared in a mortar to a uniform particle size distribution. Silicon powder (-325 mesh) was added to all powder samples as an internal standard to correct for any systematic error. X-ray diffraction analysis of the samples was carried out using X'PertHighScore Plus software in combination with Rietveld analysis and Pearson's crystal database[47].

Secondary dendrite arm spacing was measured using the linear intercept method from optical micrographs. Suitable locations were selected where secondary dendrite arms are clearly distinguishable. Then the average secondary dendrite arm spacing was measured by counting the number of arms intercepting a straight line of a known length. Readings were taken at 10 different locations close to the thermocouple position in the wedge and then averaged.

## 5. Results and discussion

### 5.1 Thermal analysis

The cooling curves obtained at different locations of the wedge cast samples were analyzed to obtain important thermal parameters. A cooling curve contains information regarding the release of heat during solidification. This release of heat eventually changes the slope of the cooling curve which indicates the characteristics of transformation and phase reactions during solidification. However, the amount of the heat evolved during some phase transformations is ~~so~~ very small that it is difficult to detect these changes from the cooling curve alone. Hence, the first and second derivative of the cooling curve was employed to determine these thermal parameters accurately. This procedure is presented in Figure 3 for location 1 of AZ91D alloy. The block arrows denote the approximate start and end of solidification as determined from temperatures at deviations from linearity in the first and second derivative curves. The results are summarized in Table 3. The liquidus and solidus temperatures recorded at different wedge locations ~~did not follow any increasing or decreasing trend~~ remain constant with regardless the change of cooling rate. From Table 3, it can be seen that the rare earth containing alloys have the smallest solidification range.

~~Cooling-~~ The cooling rates of the three investigated alloys at different thermocouple locations are presented in Table 4. For ease of calculation and representation, cooling rates were considered to be changing linearly within the approximate solidification range of the alloys. A little difference

in cooling rates among the first three locations was noticed. Although it is considered that cooling rate decreases gradually from location 1 to 6, it is evident from the table that for all three alloys, the cooling rate at location 2 is slightly higher than location 1. The deviation observed at these thermocouple locations can possibly be explained by some phenomenological factors. Firstly, this could be due to the delay in thermocouple response to correctly record the temperature change in rapidly cooled locations. Secondly, the pattern of mold filling might also be responsible. The wedge cast sample is very narrow at the bottom hence this narrow end could solidify much earlier, before the rest of the locations. But the molten metal on top of this solidified location will affect its cooling rate. Thirdly, this thin end at the bottom of wedge might not be cooled properly by the circulating cooling water due to stagnation. However, samples with the same cooling rate might have different amounts of microsegregation based on cooling and solidification conditions such as thickness of sample, coarsening, and homogenization period.

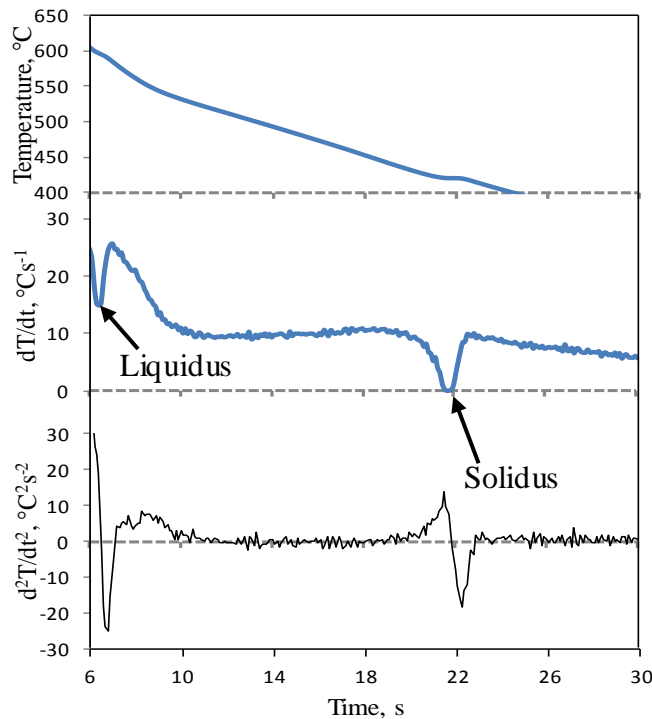


Figure 3: The cooling, first and second derivative curves of the AZ91D alloy showing the solidus and liquidus

Table 3: Liquidus, solidus and freezing range calculation of the three alloys

Alloy	Liquidus(°C)	Solidus(°C)	Freezing range(°C)
AZ91D	600	410	190
AM60B	620	415	205
AE44	630	575	55

Table 4: Cooling rate of investigated alloys within the solidification range

Cooling rate °C/s
-------------------


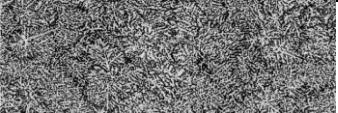
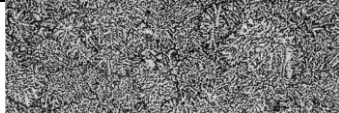
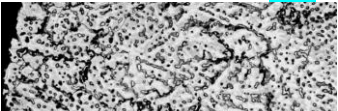
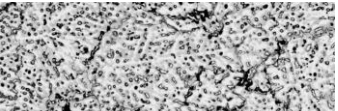
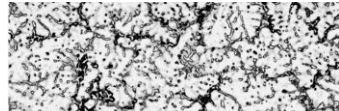
Location	AZ91D (600°C-410°C)	AM60B (620°C-415°C)	AE44 (630°C-575°C)
1	10.11	16.13	6.05
2	11.32	16.55	7.79
3	11.41	16	7.26
4	10.15	11.87	5.84
5	8.08	8.17	3.01
6	5.18	5.02	1.49

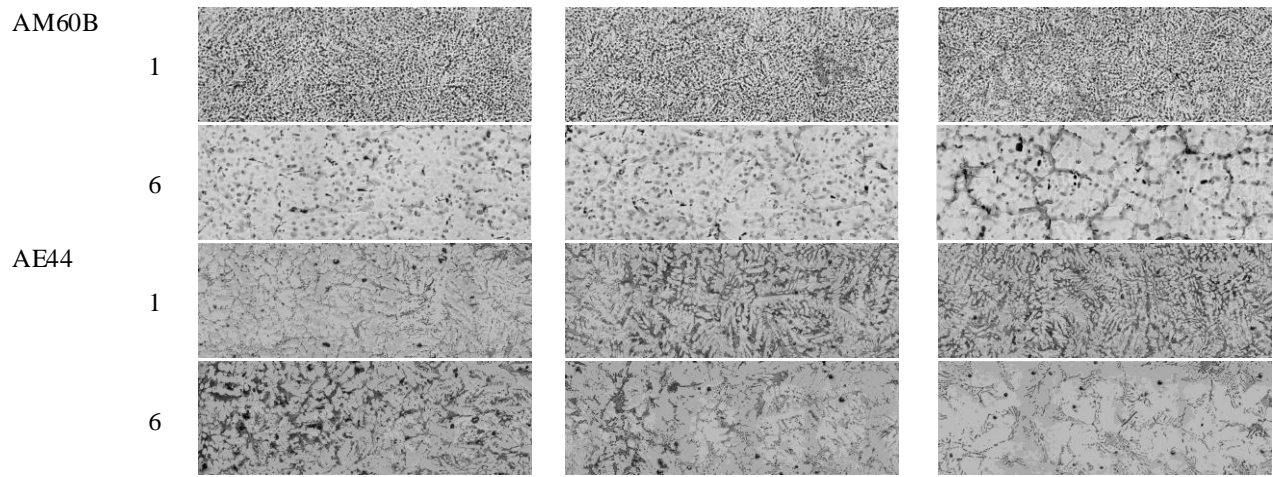
## 5.2 Microstructural analysis

The microstructure of the three studied magnesium alloys was characterized **by** quantifying the area percentage of **the** secondary phases, average size of the secondary phase particles, **the** maximum size of the secondary phase particles and **the** secondary dendrite arm spacing. All these microstructural features vary significantly with the change in cooling rate and subsequent microsegregation. The BSE micrographs were taken at 500X magnification for image analysis and each micrograph covers an area of 227 $\mu$ m $\times$ 200 $\mu$ m. Measurement of average and maximum size of secondary phase particles at specific locations provides information regarding overall particle size distribution.

Microstructural mapping was done from **the** edge to edge for the first four thermocouple positions. For locations 5 and 6, as they are much wider, pictures were taken from the center to the edge of the wedge instead of the regular patterned edge to edge. Microstructural maps and important segments are shown in Table 5. For each location of the wedge, these merged micrographic maps are divided into three sections, edge, transition from columnar to equiaxed, and mid position of the wedge.

**Table 5: Microstructural mapping of AZ91D, AM60B and AE44 alloys and their details in locations 1 and 6. The pictures were taken at magnification of 100X**

Alloy	Location	Details		
		Edge of the wedge	Columnar to equiaxed transition	Center of the wedge
AZ91D	1			
	6			



The general microstructure of the as-cast Mg alloys is demonstrated in Figure 4. AZ91D alloy is characterized by a solid solution of aluminum in magnesium, which is known as  $\alpha$ -Mg (hexagonal close packed structure) and eutectic  $\beta$ -Mg<sub>17</sub>Al<sub>12</sub> phase. Dendrite arms of  $\alpha$ -Mg are surrounded by a eutectic mixture of  $\alpha$  and  $\beta$ -Mg<sub>17</sub>Al<sub>12</sub>. In addition to this, a small amount of Al<sub>8</sub>Mn<sub>5</sub> is also noticed within the  $\alpha$ -Mg matrix. These phases are shown in Figure 4(a). The  $\beta$ -Mg<sub>17</sub>Al<sub>12</sub> phase may be fully or partially divorced depending on the solidification rate. The typical microstructure of AM60B alloy consisting of  $\alpha$ -Mg dendrite cells and a divorced-eutectic ( $\alpha$ -Mg+ $\beta$ -Mg<sub>17</sub>Al<sub>12</sub>) is presented in Figure 4 (b). A few spherical Mn-rich intermetallic particles are also generally observed in the microstructure. The primary  $\alpha$ -Mg dendrites that form the largest portion of the microstructure, are surrounded by ~~the~~ divorced eutectic. A typical microstructure of AE44 alloy consisting of primary  $\alpha$ -Mg dendrites and intermetallic phases in the interdendritic regions or at grain boundaries is presented in Figure 4 (c). The intermetallic phases have two distinctive morphologies; one is a lamellar or needle-like acicular morphology and the other with a particulate or globular shape. The lamellar phase is identified as Al<sub>11</sub>RE<sub>3</sub> and the particulate shaped is particles are Al<sub>3</sub>RE. Al<sub>11</sub>RE<sub>3</sub> is the dominant phase in all wedge locations; the presence of Al<sub>3</sub>RE is in very small amounts.

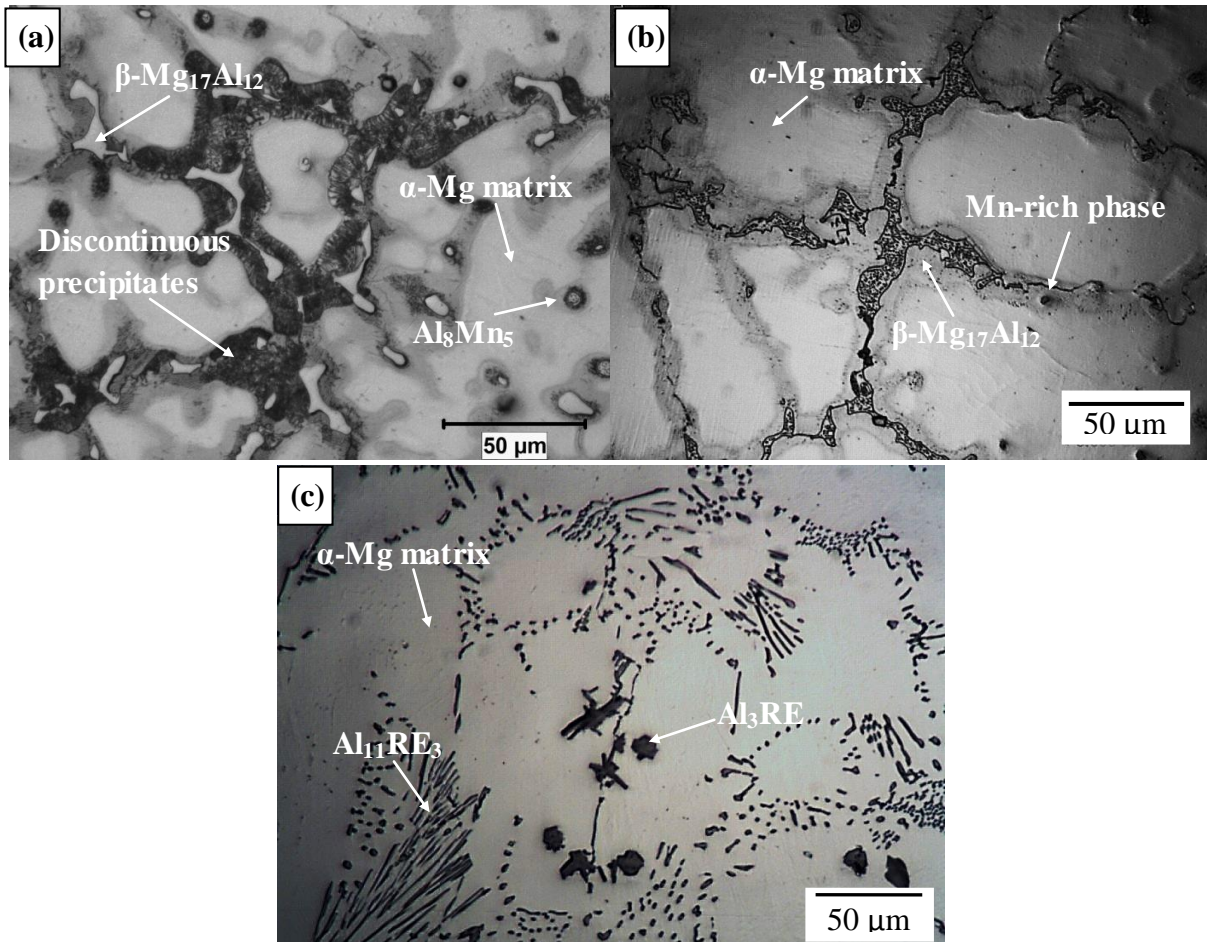


Figure 4: ~~Microstructure~~ General microstructure of the as-cast (a) AZ91D alloy; (b) AM60B; (c) AE44, regardless the thermocouple location

Figure 5 shows SEM micrographs of the mid positions of the wedge at locations 1 and 6 of the three Mg alloys.

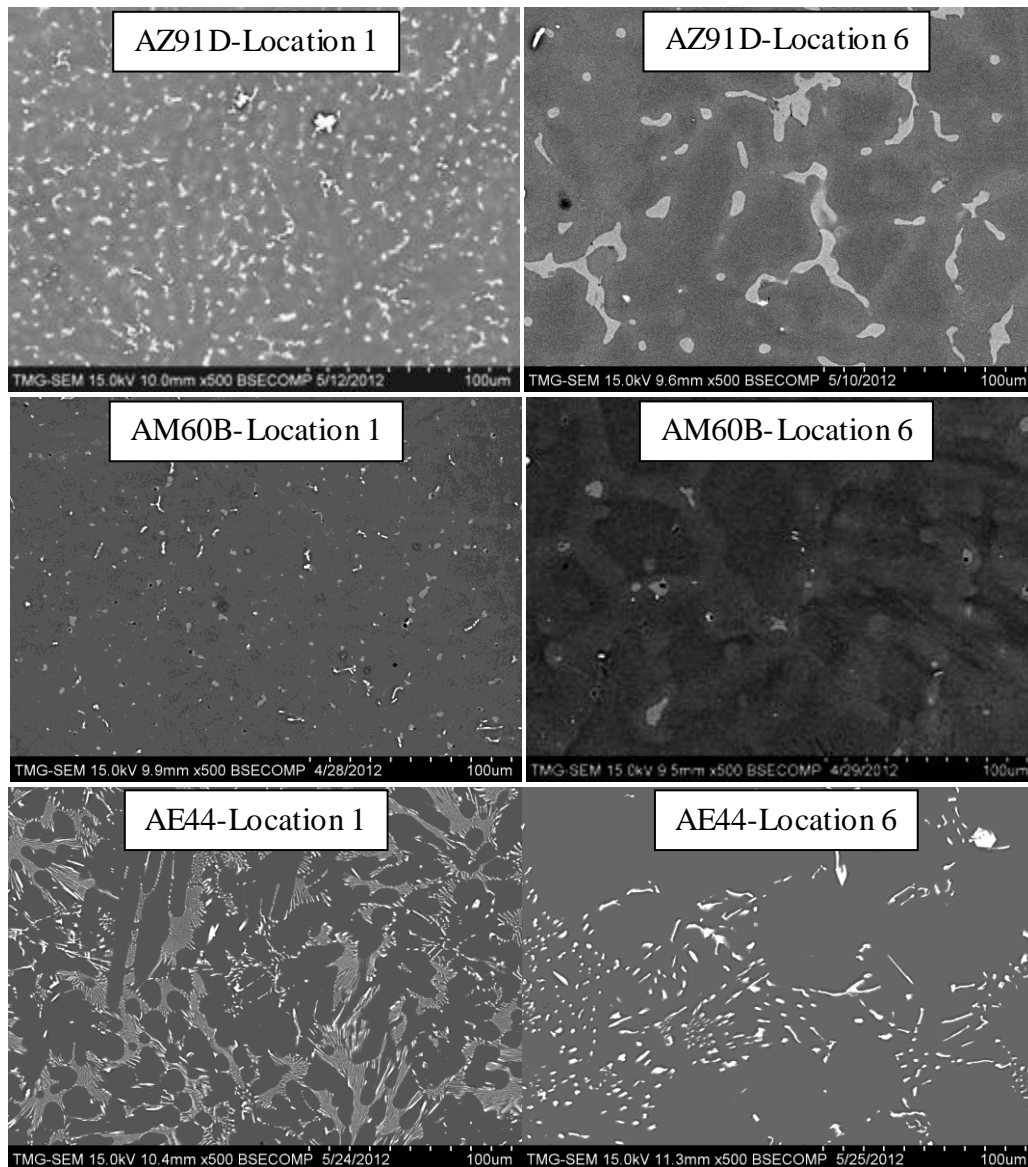


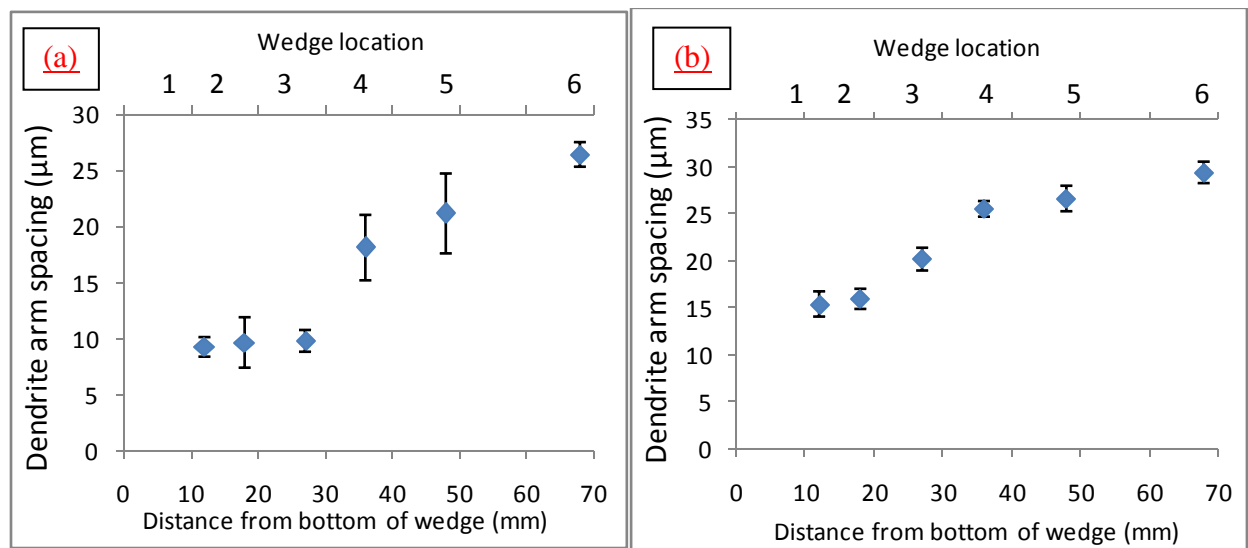
Figure 5: Microstructures at the mid position of the wedge at locations 1 and 6 for AZ91D, AM60B and AE44 alloys

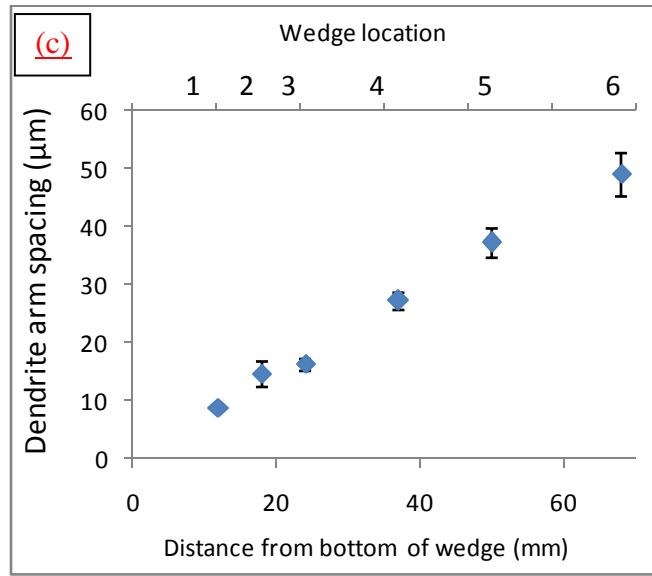
For AZ91D alloy, the size of the secondary phase particles increases significantly from location 1 to location 6. ~~Though-Although~~ the sizes of the particles are much smaller in location 1, the ~~ir~~ number ~~of nucleation sites~~ is much greater in comparison to location 6. The distance between eutectic  $\beta$ -Mg<sub>17</sub>Al<sub>12</sub> phase particles also increases with the decrease of cooling rate, which indicates that secondary dendrite arm spacing is varying with cooling rate. For AM60B, a fully divorced morphology was observed for the  $\beta$ -Mg<sub>17</sub>Al<sub>12</sub> phase in all locations. The ~~P~~ presence of coring was more obvious in locations 5 and 6. The ~~S~~ size of individual secondary phase particles increased significantly from location 1 to location 6, subsequently the number of ~~nucleation sites~~ these particles decreased. For AE44 alloy, locations 1, 2 and 3 have a similar



cluster like morphology of  $Al_{11}RE_3$ . Then from location 4, the space between the clusters starts to increase and disperse. This transition continues in location 5 and 6, where the morphology is fully dispersed and shows scattered clusters.

The variation in secondary dendrite arm spacing (SDAS) ~~was~~ measured close to the six thermocouple locations for the three Mg alloys is shown in Figure 6 (a-c). The variation of SDAS with the change of cooling rate for the three Mg alloys was calculated. It is concluded that the secondary dendrite arm spacing increases as the cooling rate decreases, from around  $9\mu m$  at location 1 up to about  $26\mu m$  in location 6, for AZ91D alloy. For AM60B alloy, the SDAS increased gradually with ~~the~~ decrease of in cooling rate, from  $15\mu m$  at location 1 up to  $30\mu m$  at location 6. The SDAS variation, for AE44, was in the range of  $10-15\mu m$  at location 1 and increased up to  $45\mu m$  at location 6, due to significant reduction in cooling rate.



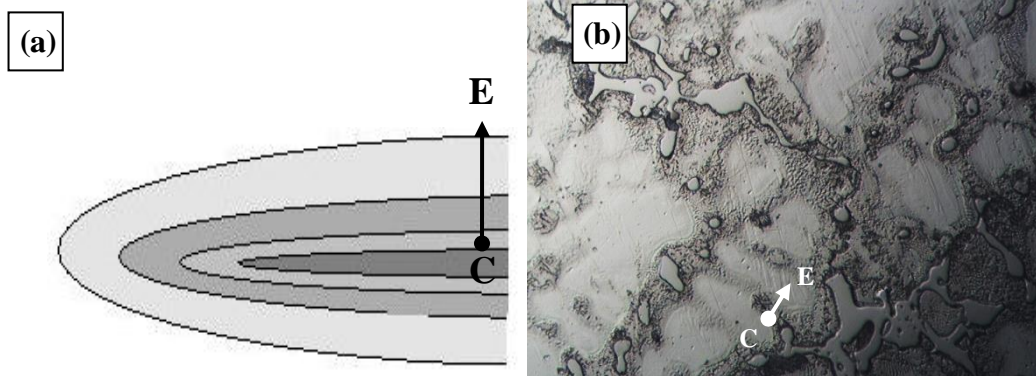


**Figure 6: Secondary dendritic arms spacing measured at center of the wedge of (a) AZ91D; (b) AM60B; (c) AE44 at different locations**

### 5.3 Microsegregation measurements

Quantitative microsegregation analysis was carried out close to the six thermocouple locations for the three investigated magnesium alloys. The following results were obtained from the acquired data at different locations of the wedge: solute redistribution profile for alloying elements (experimental & modeling), partition coefficient, segregation index (ratio between minima and bulk composition) and segregation deviation parameter ( $\sigma_m$ ), and area percentage of eutectic from the distribution profiles. Inhomogeneous distribution of solute elements during dendritic solidification of an alloy takes place due to coring. Coring or layered structure solidification is the key concept for understanding microsegregation. As can be seen from the schematic diagram of a dendrite arm in Figure 7(a), the chemical composition at point ‘C’ is different from the chemical composition of point ‘E’. It is assumed that, solidification starts at point ‘C’ and finishes at point ‘E’ and the change in chemical composition is gradual. In Figure 7 (b), the optical micrograph of AZ91D alloy is presented to compare with the schematic diagram. When the molten alloy starts to solidify, at point ‘C’ the wt% of aluminum can be as low as 2 or 3wt%, depending on the cooling rate. And it gradually increases to the last point to be solidified, namely point ‘E’. Some alloying elements have the-a tendency to accumulate in higher concentration at the edge of the dendritic arm. These elements have low concentration at the center of the arm. Some alloying elements behave in the opposite way; they have higher

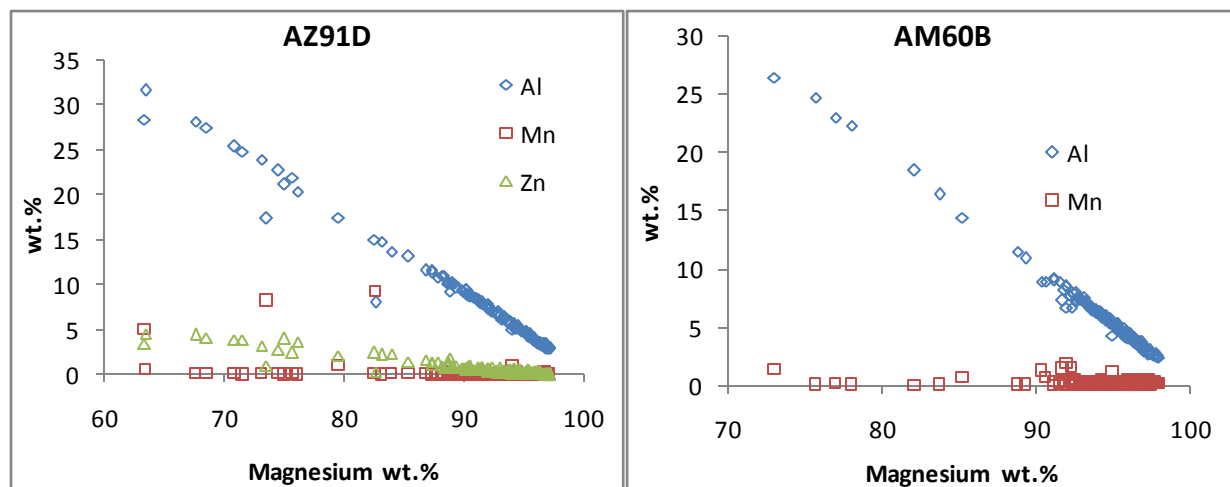
concentration at the middle of dendrite arm and then gradually decrease towards the edge. This was mainly reported for the elements forming peritectic systems.



**Figure 7: Coring in dendritic solidification; (a) schematic of dendrite arm (b) dendritic microstructure in optical micrograph of AZ91D alloy**

### 5.3.1 Solute redistribution

In this work, microsegregation measurements were performed using SEM/EDS. 150 readings were taken in a 10×15 regular grid, with a spacing of 10µm between each point. All the data points were sorted based on the weighted interval ranking sort (WIRS) method[31]. The alloying elements which were present in less than 0.5wt% in the bulk composition of the alloy were neglected, because they are below the EDS detection limit. This could be the major source of the experimental errors, which lead to provide different values of the calculated parameters. Thus In this work, the microsegregation analysis was carried out for aluminum and zinc in AZ91D, aluminum and manganese in AM60B, and aluminum, cerium, and lanthanum in AE44. Segregation The segregation trend of these alloys are for all locations in the casting is presented in Figure 8.



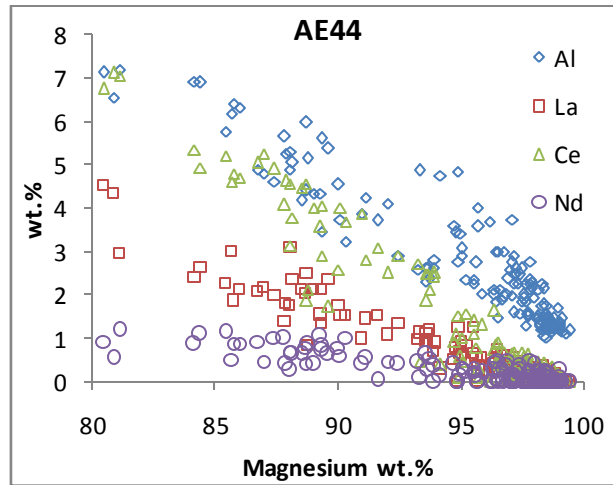


Figure 8: Segregation trend in investigated alloys

For AZ91D and AM60B, with the increase of magnesium concentration, the concentration of Al and Zn decreases while Mn shows the opposite trend. That means, Al and Zn would be low in the dendrite core and gradually increase towards the dendrite periphery. For AE44 alloy, with the increase of Mg concentration, all other elements Al, La, Ce, and Nd decrease in concentration. Thus, the concentration of these elements will be low in the dendrite core.

The Brody-Fleming equation [35] was used for modeling the solute redistribution profile modeling. ~~The Brody-Fleming equation is represented as:~~

$$C_s = KC_0 [1 - (1 - 2\alpha K) f_s]^{(K-1)/(1-2\alpha K)}$$

The parameters needed to calculate the solute profiles, (composition at any specific point solidified  $C_s$ ) using this model are dimensionless parameter  $\alpha$ , solid fraction  $f_s$ , partition coefficient  $K$ , and bulk composition  $C_0$ . ~~Secondary-The secondary~~ dendrite arm spacing and solidification time at each location was used from the experimental data to calculate  $\alpha$ . From the experimentally measured data sorted in-by the WIRS method, values of  $C_s$  and  $f_s$  can be obtained. Putting these values in the Scheil equation (Equation 2)~~provided below~~, values of the partition coefficient  $K$  ~~was-were~~ calculated.

$$C_s = K \cdot C_0 (1 - f_s)^{K-1}$$

The average value of  $K$  was then used in the Brody-Fleming model for drawing solute redistribution profiles for the three Mg alloys in all locations. These experimentally obtained values of  $K$  for all major alloying elements are listed in Table 6. From the table, it is clear that, the average value of the partition coefficient decreases with the decrease of cooling rate.

The solute redistribution profiles at locations 1 and 6, for the major alloying elements of AZ91D, AM60B and AE44 are shown in Figure 9, Figure 10 and Figure 11, respectively. Open symbols

represent the solute profile obtained from the experimental data sorted and treated through-by theWIRS method and the closed symbols represent the curves calculated using the Brody-Fleming model [35].

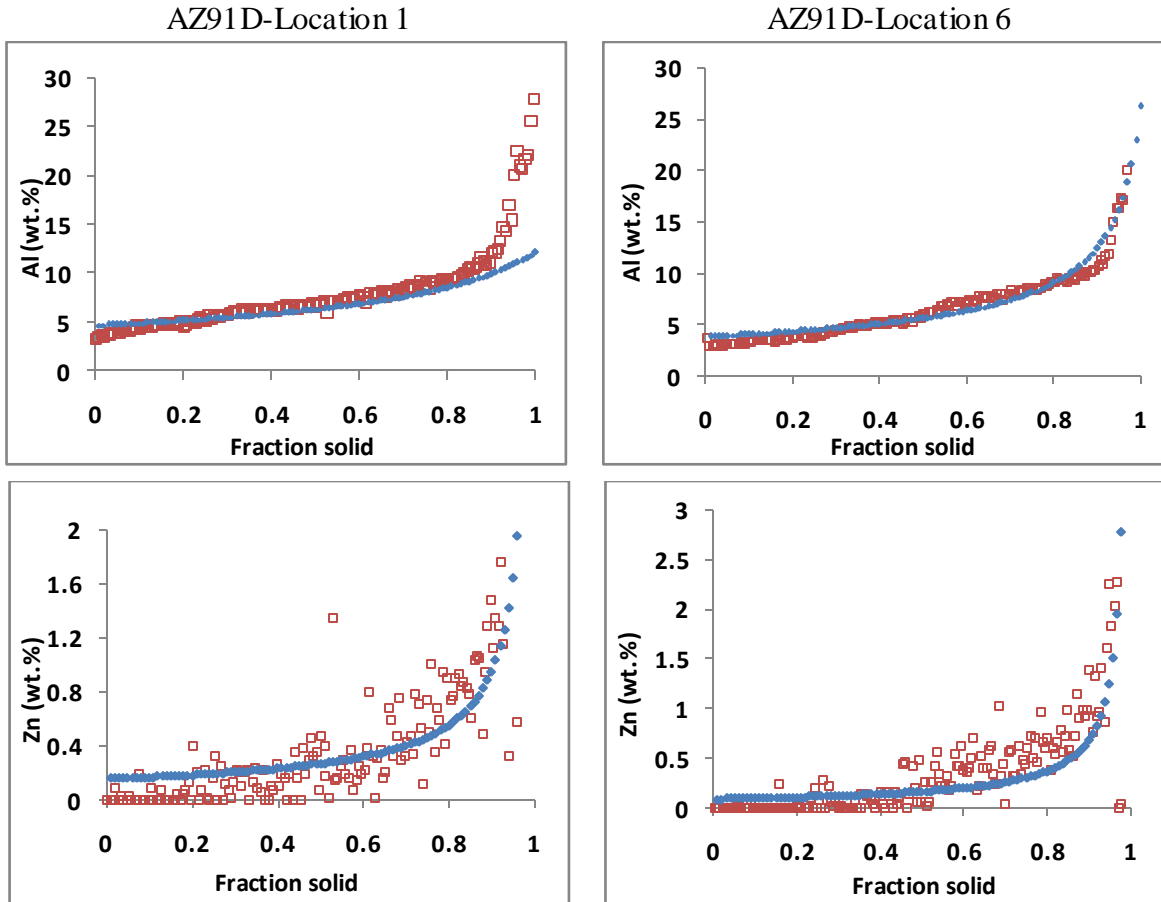
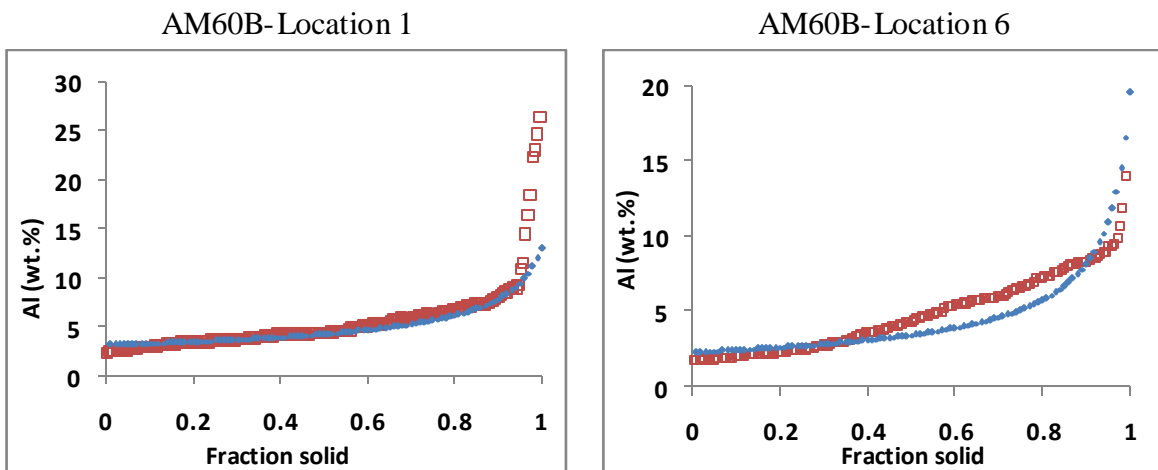


Figure 9: Solute redistribution in locations 1 and 6 of AZ91D alloy



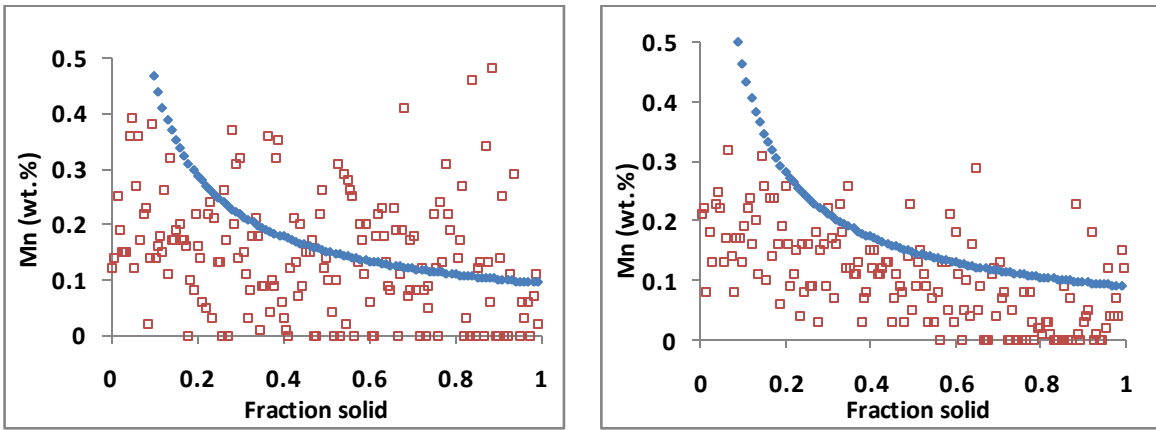
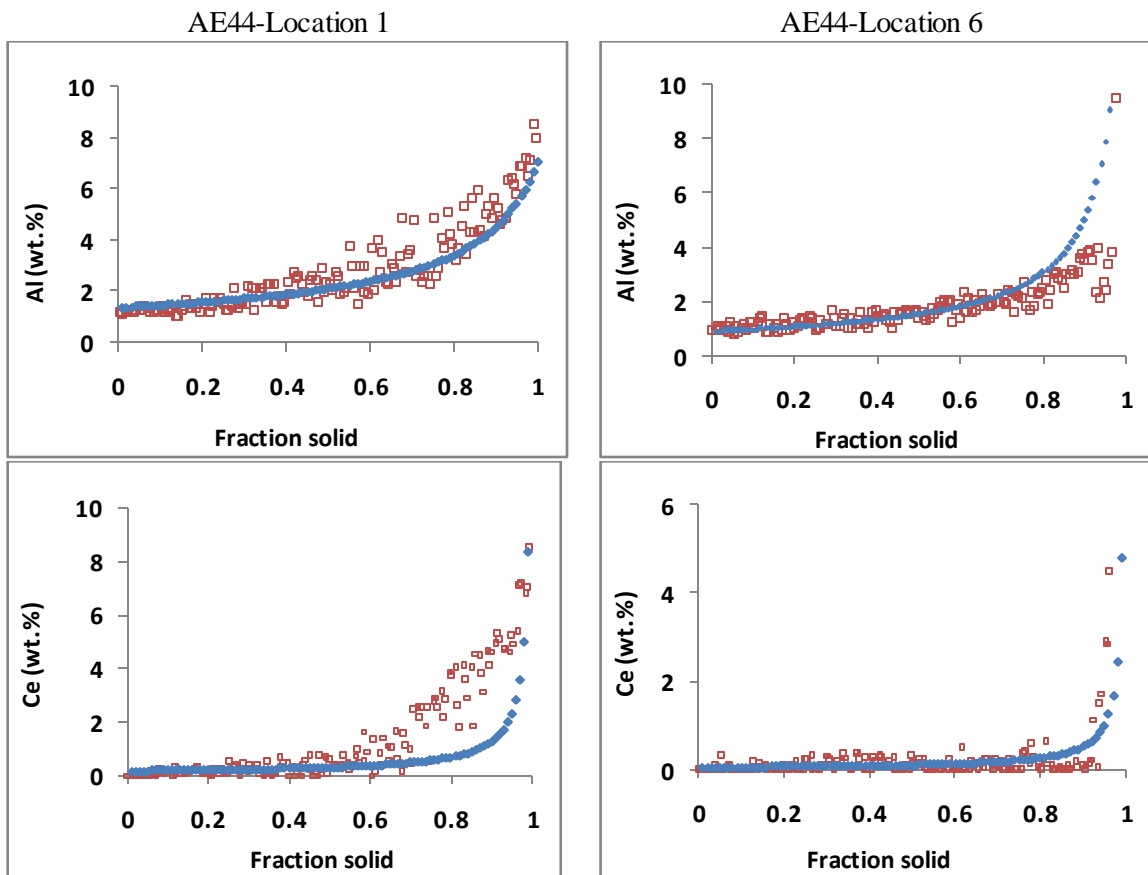


Figure 10: Solute redistribution in locations 1 and 6 of AM60B alloy



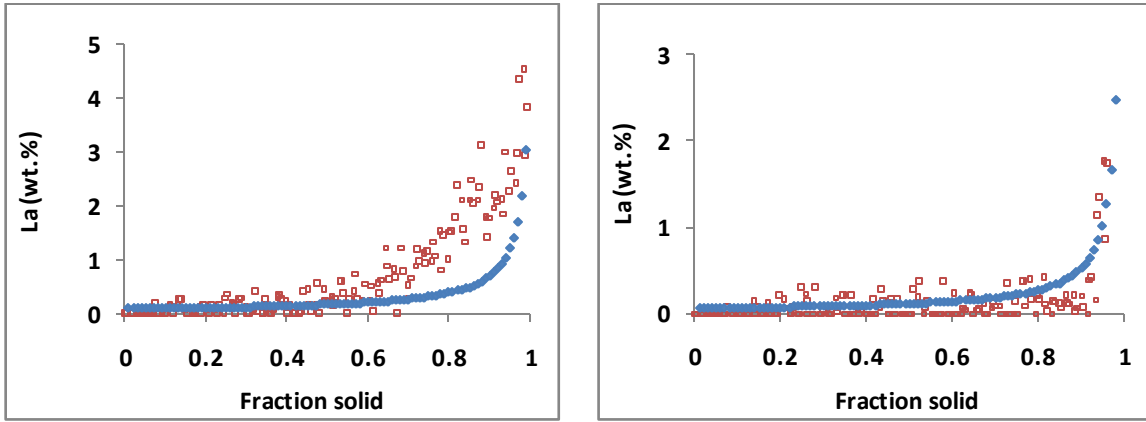


Figure 11: Solute redistribution in locations 1 and 6 of AE44 alloy

Table 6: Effective partition coefficient for major alloying elements in the investigated alloys

Location		AZ91D		AM60B		AE44		
		$K_{Al}$	$K_{Zn}$	$K_{Al}$	$K_{Mn}$	$K_{Al}$	$K_{Ce}$	$K_{La}$
1	Lowest	0.42	0.04	0.48	0.03	0.29	0.02	0.02
	Highest	0.58	0.50	0.68	0.73	0.42	0.14	0.15
	Average	<b>0.53</b>	<b>0.21</b>	<b>0.56</b>	<b>0.30</b>	<b>0.34</b>	<b>0.07</b>	<b>0.08</b>
2	Lowest	0.42	0.03	0.39	0.01	0.17	0.02	0.00
	Highest	0.63	0.40	0.49	0.57	0.40	0.18	0.22
	Average	<b>0.51</b>	<b>0.15</b>	<b>0.46</b>	<b>0.33</b>	<b>0.30</b>	<b>0.06</b>	<b>0.05</b>
3	Lowest	0.44	0.08	0.36	0.03	0.31	0.02	0.02
	Highest	0.70	0.40	0.60	0.52	0.54	0.10	0.10
	Average	<b>0.57</b>	<b>0.19</b>	<b>0.45</b>	<b>0.29</b>	<b>0.40</b>	<b>0.05</b>	<b>0.05</b>
4	Lowest	0.32	0.06	0.30	0.01	0.21	0.01	0.01
	Highest	0.56	0.36	0.47	0.23	0.33	0.13	0.07
	Average	<b>0.41</b>	<b>0.18</b>	<b>0.36</b>	<b>0.11</b>	<b>0.27</b>	<b>0.03</b>	<b>0.04</b>
5	Lowest	0.29	0.01	0.35	0.02	0.29	0.01	0.01
	Highest	0.44	0.25	0.51	0.54	0.36	0.07	0.08
	Average	<b>0.39</b>	<b>0.10</b>	<b>0.40</b>	<b>0.28</b>	<b>0.33</b>	<b>0.03</b>	<b>0.03</b>
6	Lowest	0.33	0.03	0.31	0.01	0.19	0.01	0.02
	Highest	0.56	0.29	0.55	0.62	0.25	0.05	0.05
	Average	<b>0.43</b>	<b>0.12</b>	<b>0.41</b>	<b>0.29</b>	<b>0.23</b>	<b>0.03</b>	<b>0.03</b>

\*\*Using Factsage software:  $K_{Al}=0.35$ ,  $K_{Zn}=0.09$ ,  $K_{Ce}=0.0193$ ,  $K_{La}=0.036$ ,  $K_{Mn}=1.10$

For AZ91D, the average value of  $K_{Al}$  at location 1 is 0.53 and at location 6 is 0.43. However, Shang et al. [48] reported  $K_{Al}=0.35$  and  $K_{Zn}=0.09$  for Scheil and equilibrium cooling. They also reported that for Scheil cooling conditions, the partition coefficient remains constant up to 0.85 fractions solid. For AM60B, the average value of  $K_{Al}$  at location 1 is 0.56 and at location 6 is

0.41. Although, in many solute redistribution models the partition coefficient value is considered to be the same for Scheil and equilibrium cooling conditions, the results obtained from these experiments ~~clearly~~ indicate that partition coefficient value changes significantly with cooling rate.

For AE44, the average value of  $K_{Al}$  at location 1 is 0.34 and at location 6 it decreases to 0.23. For, ~~cerium-Ce~~ and ~~lanthanumLa~~, the partition coefficient is too small, which it could be confirmed due to their low solubility in ~~magnesiumMg~~. For ~~ceriumCe~~, at location 1 the average K is 0.068 and 0.0257 at location 6. For ~~lanthanumLa~~, at location 1 the average is 0.075 and at location 6 the average is 0.0283. Chia et al. [49] reported the partition coefficient for La and Ce, using the binary phase diagrams of Mg-Ce and Mg-La, as 0.0193 and 0.036, respectively. Their partition coefficient values were closer to what has been obtained in slower cooling locations in this work. For both ~~cerium-Ce~~ and ~~lanthanumLa~~, at location 6 the partition coefficient is 0.03.

### 5.3.2 Area percentage calculations of secondary phases

According to the Mg-Al binary phase diagram, the maximum solubility of Al in Mg is around 12.9 wt.%. On the basis of this assumption, the area fraction of  $\beta$ -Mg<sub>17</sub>Al<sub>12</sub> phase was measured using the solute redistribution curve of aluminum at different wedge locations for AZ91D and AM60B alloys. In this method, a horizontal line is extended from the maximum Al solubility value. A vertical line is constructed at the end of the linear proportion of the fraction solid curve. The amount of the eutectic, then, can be calculated based on the difference between the fraction solid curve and the constructed vertical line. The procedure applied for these calculations is presented in Figure 12.



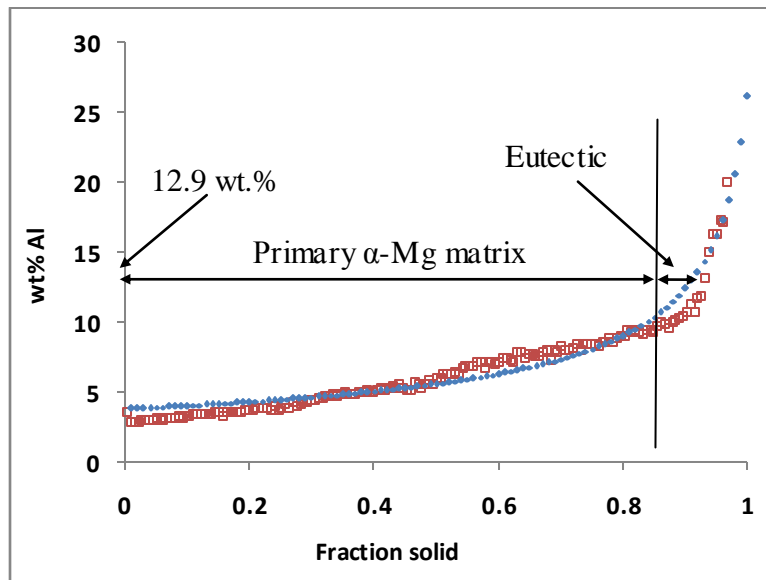


Figure 12: Procedure of for the eutectic fraction calculation using the solute redistribution curve

The eutectic area percentage was obtained, through image analysis and the solute redistribution curve of aluminum, for the three Mg alloys. In this work,  $\beta\text{-Mg}_{17}\text{Al}_{12}$  is considered the eutectic phase in the AZ91D and AM60B alloys. No eutectic phase was formed in the AE44 alloy, thus, both  $\text{Al}_3\text{RE}$  and  $\text{Al}_{11}\text{RE}_3$  were so-called secondary precipitates. Hence, for the three alloys, the  $\alpha\text{-Mg}$  matrix was considered the primary phase and all other particles were called secondary phase. The area percent distribution of secondary phases measured from the solute redistribution curve and image analysis are available in Table 7. Accordingly, the eutectic area percentage of AZ91D alloy increases with cooling rate up to location 4, then decreases at locations 5 and 6. This trend is similar to the observation of by image analysis. For AM60B, at sample locations 1, 2 and 3, the area fraction was in the range of 3.5-5%. Afterward a reduction was observed at location 5 and 6. At location 6 it was only 2%.

In AE44, the solubility composition of Al is very low in  $\alpha\text{-Mg}$  matrix, as most of the aluminum reacts with the rare earth elements to form precipitates. Solubility of La, Ce and Nd is also very low in the matrix. Hence, the maximum solid solubility of La in Mg, 0.8wt.% was assumed as the beginning of precipitate formation. For AE44 alloy, area percentage of secondary precipitates decreases gradually with cooling rate from 30% at location 1 to 8% at location 6. Hehmann et al. [50] reported that the solid solubility of Al, La, and Ce in Mg could be increased by rapid solidification method. Hence, increased solid solubility in  $\alpha\text{-Mg}$  matrix will result in lower area percentage of eutectic phases. In the present experiment, very high cooling rate was observed at locations close to bottom of the wedge, therefore it could affect the maximum solid solubility of

other alloying elements in magnesium. That means, if accurate values of solid solubility are used to calculate the area percentage, the difference between image analysis and the solute distribution curve method may become less.

**Table 7: Area percentage of secondary phases measured from solute redistribution curve and image analysis for the investigated alloys**

Location	AZ91D		AM60B		AE44	
	Solute curve	Image analysis	Solute curve	Image analysis	Solute curve	Image analysis
1	7.5	5.5	3.4	1.6	30	20.8
2	7.6	5.8	4.0	1.6	24	21.0
3	8	6.5	5.0	2.1	22	17.8
4	10	7.1	4.0	2.1	12	13.2
5	7	6.5	2.7	1.9	12	9.2
6	6.6	4.5	2.0	1.7	8	8.6

### 5.3.3 Segregation index and minimum composition

The segregation index is the ratio between the minimum composition and bulk composition of an alloying element. To determine the minimum at a specific location, the average of the ten lowest compositions were taken. The minimum concentration of aluminum and the segregation index at different wedge locations for the three alloys are presented in Table 8. From the table, it can be seen that as the cooling rate decreases, the minimum composition decreases, hence the severity of segregation increases. For AZ91D, the minimum concentration of aluminum decreases with the decrease of cooling rate. At location 1, the composition is 3.6wt.% and at location 6, it drops to 3.01 wt.%. For AM60B, at location 1, minimum concentration of aluminum is 2.5 wt.% and at location 6 it reduces to 1.8 wt.%. For AE44, at location 1, the minimum concentration of aluminum is 1.1 wt.% and at locations 6 the concentration is 0.9wt.%.

**Table 8: Minimum concentration of aluminum and segregation index for the investigated alloys at different locations**

Location	AZ91D		AM60B		AE44	
	Minimum Al	Segregation index	Minimum Al	Segregation index	Minimum Al	Segregation index
1	3.63	2.42	2.56	2.23	1.15	3.44
2	3.57	2.47	2.25	2.54	1.21	3.27
3	3.54	2.49	2.19	2.61	1.30	3.04
4	2.90	3.03	1.89	3.01	1.06	3.73
5	3.12	2.82	2.05	2.78	1.07	3.69
6	3.01	2.93	1.84	3.10	0.90	4.39

### 5.3.4 Segregation deviation

The severity of microsegregation is measured by the segregation deviation parameter ( $\sigma_m$ ) using Equation 1. Martorano et al.[29] reported that microsegregation severity is lower for columnar dendrites than for equiaxed ones. It has also been reported that the increase in segregation deviation parameter  $\sigma_m$ , for a change in structure from columnar to equiaxed seems to be constant, approximately 0.11, for the Cu-8 wt.% Sn alloys. However, this value can be applicable for any particular system, since it shows the difference in the amount of segregation between columnar and equiaxed segregation. Consequently, the type of dendritic growth seems to be an important variable to define microsegregation. The greater microsegregation severity observed in an equiaxed dendrite zone compared with that in columnar dendrites might be the result of more homogenization in the latter structure. The overall deviation from the bulk composition for aluminum is presented in Figure 13.

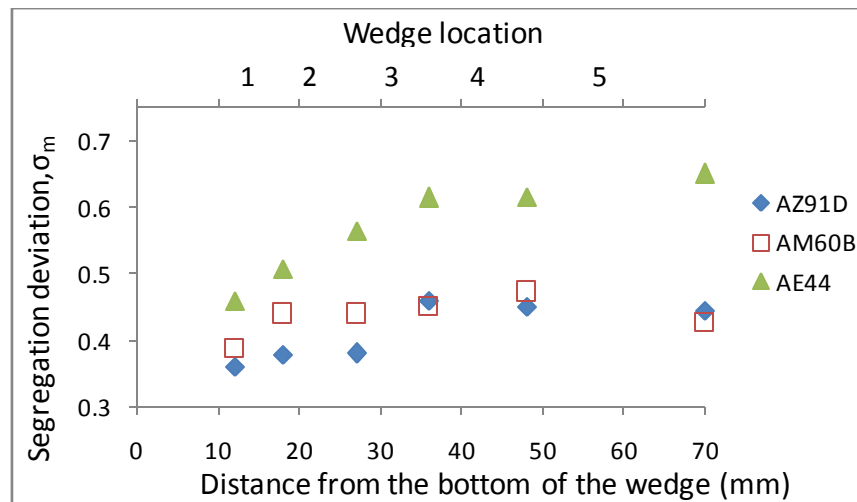


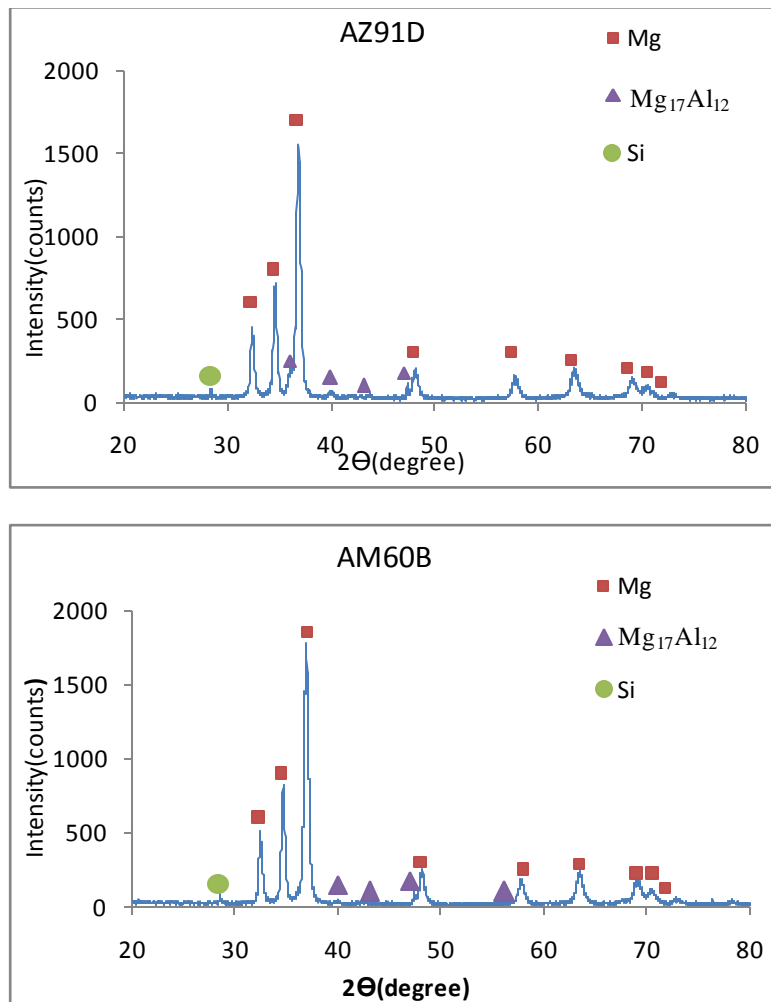
Figure 13: Segregation deviation for three investigated alloys

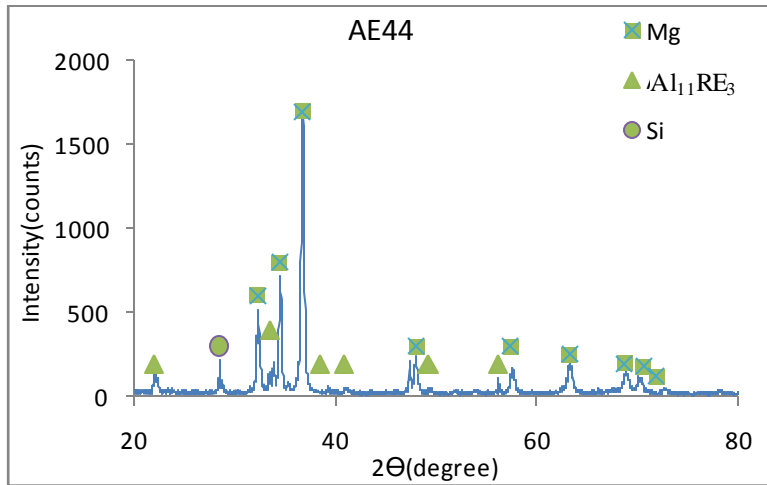
In the present work, location 1 could be considered as columnar dendritic and location 6 as equiaxed dendritic. The difference in deviation from location 1 to location 6, for AZ91D is 0.08, for AM60B is 0.06, and for AE44 it is 0.19 which is comparable to the results observed by Martorano et al.[29].

For AM60B alloy, from location 1 to location 5, the segregation deviation increases then it slightly decreases at location 6. Thus, that contradicts contradicting with the segregation index. The segregation index is high at location 6 but when the segregation deviation is calculated on a broader range the segregation deviation is comparatively lower than at other locations.

#### 5.4 XRD results

XRD patterns of these three alloys are presented in Figure 13. For AZ91D, AM60B and AE44 alloys,  $\alpha$  Mg is the dominant phase. For AZ91D and AM60B, the other phase present in a detectable amount is  $\beta$   $Mg_{17}Al_{12}$ . For AE44 alloy, other phase present is  $Al_{11}RE_3$ . Crystal structure of  $Al_{11}Ce_3$  was used to identify  $Al_{11}RE_3$  including  $Al_{11}Ce_3$  and  $Al_{11}La_3$ . Weight percentages of secondary phases at these locations were also calculated from XRD results using Rietveld method. These values are presented in Table 8. In all cases, weight percentage of the secondary phases increase with decreasing cooling rate, confirming the microstructural observations.





**Figure 13: XRD pattern for three alloys**

**Table 9: wt% of secondary phases measured by XRD analysis**

	AZ91D	AM60B	AE44
	wt% $Mg_{17}Al_{12}$	wt% $Mg_{17}Al_{12}$	wt% $Al_{11}RE_3$
Location 1	1.1±0.3	0.8±0.2	4.0±0.3
Location 2	1.4	1.0	4.0
Location 3	1.3	1.1	4.2
Location 4	2.0	1.3	4.3
Location 5	2.5	1.4	4.6
Location 6	2.6±0.4	1.4±0.3	4.4±0.5

## 6. Summary

Three main Mg alloys (AZ91D, AM60B and AE44) solidified in a range of cooling rates (1-20°C/min) were studied and found to exhibit dendritic microstructures. At higher cooling rate (location 1 and 2) the dendritic morphology was predominantly columnar and at lower cooling rate (location 5 and 6) dendritic equiaxed morphology was observed. Secondary dendrite arm spacing increased significantly with the decrease of cooling rate for all three investigated alloys. The arm spacing ranges for the different alloys are: 10 to 25 μm for AZ91D, 15 to 30 μm for AM60B, and 10 to 45 μm for AE44. The average size of secondary phase particles increased substantially with the decrease of cooling rate. For AZ91D, the  $\beta$ - $Mg_{17}Al_{12}$  phase had a partially divorced morphology at fast cooled locations of the wedge and fully divorced morphology at slowly cooled locations. For AE44, the secondary precipitates had cluster-like morphology at faster cooling rate, and gradually became more dispersed with slower cooling rate.

Microsegregation was more pronounced at slow cooled locations, which is evident from the microsegregation parameters. The minimum concentration of aluminum was always low for slow cooled locations (3wt% at location 6 in comparison to 3.6wt% at location 1 for AZ91D alloy). Significant difference in segregation deviation ( $\Delta\sigma_m$ ) was observed between the columnar and the equiaxed dendrites, approximately in the range of (0.06-0.19) for the three alloys. The higher segregation deviation observed in equiaxed morphology is probably due to prolonged back diffusion which takes place at slow cooling rates.

Experimentally obtained solute redistribution profiles match reasonably with theoretically calculated profiles except at very low solid fraction. This discrepancy at low solid fraction is possibly due to the presence of a few primary dendritic arms in the microstructure which have lower concentration of aluminum than the rest of the matrix. The elemental partition coefficients calculated from the experimentally obtained redistribution profiles were comparatively higher than the partition coefficients calculated from binary phase diagrams.

Area fraction of secondary phase particles measured by two different methods, image analysis and solute redistribution curves showed close resemblance. Area fraction measured from solute redistribution curves is comparatively higher due to the fact that in case of image analysis only the secondary phase particles are measured based on color threshold, while in solute curve method regions adjacent to particles which have high concentration of alloying elements (e.g. eutectic phases) are also taken into account.

~~Systematic quantitative microsegregation analyses were carried out for three commercially important magnesium alloys AZ91D, AM60B and AE44 using wedge casting method. Changes in microstructural and morphological features due to variation in cooling rate at different locations of the wedge casting were analyzed. Elemental analysis was carried out in the vicinity of thermocouple locations for the three alloys to obtain the microsegregation trend, solute redistribution profiles, and elemental partition coefficient. Apart from that, solute redistribution profiles were also drawn using Brody Fleming model, and were compared with the experimentally obtained curves.~~

~~For the three alloys, the area percentage of secondary phase particles was comparatively more in areas closer to the mold wall at all wedge locations. Secondary dendrite arm spacing increased gradually with the decrease of cooling rate. Average and maximum area of the secondary phase particles increased significantly with decreasing cooling rate. For AZ91D,  $\beta$  Mg<sub>17</sub>Al<sub>12</sub> phase had partially divorced morphology at fast cooled locations of the wedge and fully divorced~~

morphology at slowly cooled locations. For AE44, the secondary precipitates had cluster like morphology at faster cooling rate, and gradually became more dispersed with slower cooling rate.

Columnar to equiaxed transition was not very clear cut as it is in the case of directional solidification. In general, it can be said that at locations 1 and 2, the morphology of the dendrites were basically columnar. At locations 3 and 4, there was mixed morphology and at locations 5 and 6, fully equiaxed morphology was observed. Microsegregation was more pronounced in equiaxed morphology which is the consequence of slower cooling rate and prolonged back diffusion.

Experimentally obtained elemental partitioning coefficients and solute redistribution profiles for the major alloying elements at different cooling rates should be very important for microstructural simulation models of these alloys and for the validation of existing models, which would be of great importance for optimizing the casting procedure. Elemental partitioning coefficient of major alloying elements of the investigated alloys decreased with the decrease of cooling rate. Experimentally obtained solute redistribution profiles matched reasonably well with theoretically calculated profiles except at very low solid fraction.

## **7. Acknowledgment**

The authors would like to acknowledge AUTO21 NSERC Strategic Network of Excellence for the financial support of this work.

## References

- [1] A. Bobby, U. Pillai, B. Pillai, B. Pai, Developments in Magnesium Alloys for Transport Applications—An Overview, *Indian Foundry Journal*, 57 (2011) 30.
- [2] R.S. Beals, C. Tissington, X. Zhang, K. Kainer, J. Petrillo, M. Verbrugge, M. Pekguleryuz, Magnesium global development: Outcomes from the TMS 2007 annual meeting, *Journal of the Minerals, Metals and Materials Society*, 59 (2007) 39-42.
- [3] G. Davies, *Materials for automobile bodies*, Butterworth-Heinemann, Oxford, 2003.
- [4] H. Mao, V. Chandrasekar, M. Murray, C. Mobley, D. Rodrigo, R. Esdaile, J. Brevick, Microstructural characteristics of die cast AZ91D and AM60 magnesium alloys, SAE, 1996.
- [5] E. Aghion, B. Bronfin, D. Eliezer, The role of the magnesium industry in protecting the environment, *Journal of Materials Processing Technology*, 117 (2001) 381-385.
- [6] J. Quaresma, C. Santos, A. Garcia, Correlation between unsteady-state solidification conditions, dendrite spacings, and mechanical properties of Al-Cu alloys, *Metallurgical and Materials Transactions A*, 31 (2000) 3167-3178.
- [7] X. Zheng, A. Luo, C. Zhang, J. Dong, R. Waldo, Directional Solidification and Microsegregation in a Magnesium-Aluminum-Calcium Alloy, *Metallurgical and Materials Transactions A*, 43 (2012) 3239-3248.
- [8] D. Mirković, R. Schmid-Fetzer, Directional Solidification of Mg-Al Alloys and Microsegregation Study of Mg Alloys AZ31 and AM50: Part I. Methodology, *Metallurgical and Materials Transactions A*, 40 (2009) 958-973.
- [9] D. Mirković, R. Schmid-Fetzer, Directional Solidification of Mg-Al Alloys and Microsegregation Study of Mg Alloys AZ31 and AM50: Part II. Comparison between AZ31 and AM50, *Metallurgical and Materials Transactions A*, 40 (2009) 974-981.
- [10] C. Zhang, D. Ma, K.S. Wu, H.B. Cao, G.P. Cao, S. Kou, Y.A. Chang, X.Y. Yan, Microstructure and microsegregation in directionally solidified Mg-4Al alloy, *Intermetallics*, 15 (2007) 1395-1400.
- [11] A. Luo, Understanding the solidification of magnesium alloys, in: *Proceedings of the Third International Magnesium Conference*, Manchester, UK, 1997, pp. 449–464.
- [12] D.H. StJohn, A.K. Dahle, T. Abbott, M.D. Nave, M. Qian, Solidification of cast magnesium alloys, in: *Proceedings of the Minerals, Metals and Materials Society (TMS), Magnesium Technology*, San Diego, CA, 2003, pp. 95–100.



- [13] Y.W. Riddle, M.M. Makhlof, Characterizing solidification by non- equilibrium thermal analysis, in: Proceedings of the Minerals, Metals and Materials Society (TMS), Magnesium Technology, San Diego, CA, 2003, pp. 101–106.
- [14] A. Lindemann, J. Schmidt, M. Todte, T. Zeuner, Thermal analytical investigations of the magnesium alloys AM60 and AZ91 including the melting range, *Thermochimica Acta*, 269 (2002) 381-382.
- [15] M. Ohno, D. Mirkovic, R. Schmid-Fetzer, On liquidus and solidus temperature in AZ and AM alloys, in: Proceedings of the Minerals, Metals and Materials Society (TMS), San Antonio, TX, 2006, pp. 129–132.
- [16] M.D. Nave, A.K. Dahle, D.H. StJohn, Eutectic growth morphologies in magnesium-aluminum alloys, in: Proceedings of the Minerals, Metals and Materials Society (TMS), Nashville, TN, 2000, pp. 233–242.
- [17] L.P. Barber, Characterization of the solidification behavior and resultant microstructures of magnesium-aluminum alloys, in: Materials Science and Engineering, Worcester Polytechnic Institute, Worcester, MA, 2004.
- [18] A.K. Dahle, Y.C. Lee, M.D. Nave, P.L. Schaffer, D.H. StJohn, Development of the as-cast microstructure in magnesium-aluminium alloys, *Journal of Light Metals*, 1 (2001) 61-72.
- [19] S. Barbagallo, H. Laukli, O. Lohne, E. Cerri, Divorced eutectic in a HPDC magnesium-aluminum alloy, *Journal of Alloys and Compounds*, 378 (2004) 226-232.
- [20] M.N. Khan, M. Aljarrah, J.T. Wood, M. Medraj, The effect of cooling rate on thermophysical properties of magnesium alloys, *Journal of Materials Research*, 26 (2011) 974-982.
- [21] L.-Y. Wei, R. Warren, Microstructural characterisation of several magnesium alloys in AM series, *Materials Science and Technology*, 23 (2007) 745-752.
- [22] Q. Han, E. Kenik, S. Agnew, S. Viswanathan, Solidification behaviour of commercial magnesium alloys; *Magnesium Technology 2001*, 11.-15.02. 2001, New Orleans, The Minerals, Metals & Materials Society, Warrendale, S, (2001) 81-86.
- [23] Z. Zhang, A. Couture, R. Tremblay, D. Dube, Microstructure and mechanical properties of permanent mold and die casting of AZ 91 magnesium alloy, in: *Light metals-proceedings-Canadian Inst of Mining, Metallurgy and Petroleum*, 1999, pp. 397-406.
- [24] A. Ditze, K. Schwerdtfeger, Strip casting of magnesium with the single belt process, *Scandinavian journal of metallurgy*, 32 (2003) 311-316.

- [25] S. Guo, Q. Le, Y. Han, Z. Zhao, J. Cui, The effect of the electromagnetic vibration on the microstructure, segregation, and mechanical properties of As-cast AZ80 magnesium alloy billet, *Metallurgical and Materials Transactions A*, 37 (2006) 3715-3724.
- [26] M. Gungor, A statistically significant experimental technique for investigating microsegregation in cast alloys, *Metallurgical and Materials Transactions A*, 20 (1989) 2529-2533.
- [27] J. Sarreal, G. Abbaschian, The effect of solidification rate on microsegregation, *Metallurgical and Materials Transactions A*, 17 (1986) 2063-2073.
- [28] M.C. Flemings, D.R. Poirier, R.V. Barone, H.D. Brody, Microsegregation in Iron Base Alloys, *Journal of Iron and steel institute*, 208 (1970) 371-381.
- [29] M. Martorano, J. Capocchi, Effects of processing variables on the microsegregation of directionally cast samples, *Metallurgical and Materials Transactions A*, 31 (2000) 3137-3148.
- [30] W. Yang, K.-M. Chang, W. Chen, S. Mannan, J. DeBarbadillo, Monte carlo sampling for microsegregation measurements in cast structures, *Metallurgical and Materials Transactions A*, 31 (2000) 2569-2574.
- [31] M. Ganesan, D. Dye, P. Lee, A technique for characterizing microsegregation in multicomponent alloys and its application to single-crystal superalloy castings, *Metallurgical and Materials Transactions A*, 36 (2005) 2191-2204.
- [32] D.R. Poirier, Microsegregation in ternary iron-carbon-chromium alloys, in: Department of Metallurgy, MIT, Cambridge, MA, 1966.
- [33] E. Scheil, Bemerkungen zur schichtkristallbildung, *Zeitschrift Metallkunde*, 34 (1942) 70-72.
- [34] T. Clyne, W. Kurz, Solute redistribution during solidification with rapid solid state diffusion, *Metallurgical and Materials Transactions A*, 12 (1981) 965-971.
- [35] T. Bower, H. Brody, M. Flemings, Measurements of solute redistribution in dendritic solidification, *Transaction of the Metallurgical Society of AIME*, 236 (1966) 624-633.
- [36] I. Ohnaka, Mathematical analysis of solute redistribution during solidification with diffusion in solid phase, *Transactions of the Iron and Steel Institute of Japan*, 26 (1986) 1045-1051.
- [37] S. Kobayashi, A Mathematical Model for Solute Redistribution during Dendritic Solidification, *Transactions of the Iron and Steel Institute of Japan*, 28 (1988) 535-542.

- [38] L. Nastac, D.M. Stefanescu, An analytical model for solute redistribution during solidification of planar, columnar, or equiaxed morphology, *Metallurgical Transactions A*, 24 (1993) 2107-2118.
- [39] J. Lacaze, P. Benigni, A. Howe, Some Issues Concerning Experiments and Models for Alloy Microsegregation, *Advanced Engineering Materials*, 5 (2003) 37-46.
- [40] T. Kraft, M. Rettenmayr, H. Exner, An extended numerical procedure for predicting microstructure and microsegregation of multicomponent alloys, *Modelling and Simulation in Materials Science and Engineering*, 4 (1996) 161-177.
- [41] F.Y. Xie, T. Kraft, Y. Zuo, C.H. Moon, Y.A. Chang, Microstructure and microsegregation in Al-rich Al-Cu-Mg alloys, *Acta Materialia*, 47 (1999) 489-500.
- [42] Q. Du, A. Jacot, A two-dimensional microsegregation model for the description of microstructure formation during solidification in multicomponent alloys: Formulation and behaviour of the model, *Acta Materialia*, 53 (2005) 3479-3493.
- [43] W.J. Boettinger, U.R. Kattner, D.K. Banerjee, Analysis of solidification path and microsegregation in multicomponent alloys, in: Thomas BG, Beckermann C. *Modelling of Casting, Welding and Advanced Solidification Processes-VIII (1)*, Warrendale, PA: TMS, 1998, pp. 159-170.
- [44] M.C. Flemings, *Solidification Processing*, McGraw-Hill, 1974.
- [45] M.C. Flemings, Solidification processing, *Metallurgical and Materials Transactions B*, 5 (1974) 2121-2134.
- [46] R.M. Kearsey, Compositional effects on microsegregation behaviour in single crystal superalloy systems, in: *Mechanical and aerospace engineering*, Carleton University, Ottawa, Ontario, 2004.
- [47] H. Putz, K. Brandenburg, Pearson's Crystal Data, Crystal Structure Database for Inorganic Compounds, in, pp. CD-ROM software version.
- [48] S. Shang, H. Zhang, S. Ganeshan, Z.-K. Liu, The development and application of a thermodynamic database for magnesium alloys, *Journal of the Minerals, Metals and Materials Society*, 60 (2008) 45-47.
- [49] T.L. Chia, M.A. Easton, S.M. Zhu, M.A. Gibson, N. Birbilis, J.F. Nie, The effect of alloy composition on the microstructure and tensile properties of binary Mg-rare earth alloys, *Intermetallics*, 17 (2009) 481-490.

[50] F. Hehmann, F. Sommer, B. Predel, Extension of solid solubility in magnesium by rapid solidification, *Materials Science and Engineering: A*, 125 (1990) 249-265.

|

|